Journal of Power Sources 195 (2010) 3275–3283

Contents lists available at ScienceDirect

Journal of Power Sources

journal homepage: www.elsevier.com/locate/jpowsour

Steam reforming of liquid hydrocarbons over a nickel–alumina spinel catalyst

Clémence Fauteux-Lefebvre, Nicolas Abatzoglou*, Jasmin Blanchard, François Gitzhofer

Chemical and Biotechnological Engineering Department, Université de Sherbrooke, Sherbrooke, Quebec, Canada J1K 2R1

ARTICLE INFO

Article history:
Received 24 September 2009
Received in revised form
18 November 2009
Accepted 25 November 2009
Available online 2 December 2009

Keywords:
Steam reforming
Catalyst
Ni–alumina spinel
Diesel
Hexadecane
Propane

ABSTRACT

Interest in steam reforming of liquid hydrocarbons is growing due to the necessity of developing reliable alternatives for their use in fuel cells. In particular, solid oxide fuel cells, which can operate with mixtures of H_2 and CO, are excellent candidates for being fed with liquid fuels coming from both fossil and renewable sources. Fossil-derived, synthetic diesel is an interesting option.

In this work, an Al_2O_3–ZrO_2-supported nickel–alumina spinel was tested in a lab-scale isothermal packed-bed reactor as a catalyst of steam reforming of propane, hexadecane and tetralin as surrogates of constitutive families of all commercially available diesel fuels.

The results show that the reaction reaches equilibrium at reaction severities lower than those reported in the literature. When operated at steam excess of 250%, carbon formation is not higher than expected by theoretical thermodynamic equilibrium calculations, and no significant catalyst deactivation is observed over the test durations. Scanning electron microscopy of the fresh and used catalyst surfaces shows no significant quantities of carbon.

© 2009 Elsevier B.V. All rights reserved.

1. Introduction

In a world preoccupied by environmental threats, such as green house effect gas emissions, and high energy costs, fuel cells are promising "chemical energy-to-electricity" converters. This is mainly attributed to their higher conversion efficiency and the possibility of feeding them with fuels coming from renewable resources (i.e., green diesel).

In the case of solid oxide fuel cells (SOFC), H_2, the ideal feed can be combined with CO (i.e., syngas) without harming SOFC, which can use it as co-fuel. H_2 can be obtained from hydrocarbon reforming. The three main methods are catalytic partial oxidation (Reaction (1)), steam reforming (Reaction (2)), and auto-thermal reforming. Diesel is a good candidate for in-line H_2 production by reforming because of its high hydrogen density, already-existing distribution networks/facilities and safe storage:

$$C_nH_m + \frac{n}{2}O_2 \rightarrow nCO + \frac{m}{2}H_2 \quad (\Delta H < 0) \tag{1}$$

$$C_nH_m + nH_2O \rightarrow nCO + (n + \frac{m}{2})H_2 \quad (\Delta H > 0) \tag{2}$$

Steam reforming, studied in this paper, has the advantage of producing a higher H_2 concentration than catalytic partial oxidation. The literature reports 70–80 vol% H_2 concentration in steam reforming products whereas 35–45 vol% are the respective numbers for equivalent partial oxidation reactions [1]. The main reason is that in partial oxidation no H_2 is associated with the oxidant (O_2). In addition, partial oxidation is an exothermic reaction, and hot spots at the catalytic bed are a usual technical nuisance, which leads to higher catalyst aging rates [1].

The objective of this work was to test a new formulation (Al_2O_3–YSZ-supported $NiAl_2O_4$) in diesel steam reforming. Previous works [2–4] have disclosed that similar formulations are efficient in naphthalene and CH_4 steam or CO_2 reforming with aging resistance near that of much more expensive noble metal-based catalysts.

1.1. Reforming catalyst

Transition metals are commonly deployed for reforming reactions. Noble and non-noble metals are employed, with the first one being usually more resistant but more expensive [1,5].

There are three main causes of hydrocarbon reforming catalyst deactivation: (a) sintering, mainly produced by the surface mobility of active metals at high operating temperatures; (b) sulphur poisoning: organic sulphur contained in fossil fuels, under reforming conditions, is converted to S^{2-} which reacts with active metals at the catalyst surface. The sulphides so formed are catalytically inactive, because they prevent reactants from being adsorbed on the catalytic surface [6]; (c) coking, a term for carbon-rich compound formation and deposition. Two main undesirable reactions generate carbon deposition: Boudouard reaction (CO disproportionation to C and CO_2), and hydrocarbon cracking. Deactivation through coking is different in non-noble and noble metals, namely, metallic nickel allows carbon diffusion and dissolution which

* Corresponding author. Tel.: +1 819 821 7904; fax: +1 819 821 7955.
E-mail address: Nicolas.Abatzoglou@USherbrooke.ca (N. Abatzoglou).

0378-7753/$ – see front matter © 2009 Elsevier B.V. All rights reserved.
doi:10.1016/j.jpowsour.2009.11.121

Nomenclature

k	activation energy
N	number of moles
v_0	flow rate (mol h^{-1})
Δw	catalyst weight (g)
X	conversion
y	molar fraction

results in the formation of whisker carbon [7]. On the other hand, noble metals do not dissolve carbon significantly, culminating in less carbon formation and different carbon deposition mechanisms [7].

In diesel or other hydrocarbon reforming reactions, the catalyst is usually deactivated within 100 h of use [8–10]. Depending on the catalyst and reaction severity (mainly sufficiently low space velocities), concentrations close to theoretical thermodynamic equilibrium can be reached. Strohm et al. [10] studied the steam reforming of simulated jet fuel without sulphur and reported constant H_2 concentrations of 60 vol% for 80 h with a ceria–alumina-supported rhodium (Rh) catalyst. The reactions occurred at temperatures below 520 °C and an H_2O/C molar ratio of 3. When they added 35 ppm of sulphur in the feed, the catalyst was deactivated within 21 h.

With an Al_2O_3-supported bimetallic noble metal and a metal-loading <1.5% catalyst, Ming et al. [6] obtained constant H_2 concentrations of 70% over a 73-h steady state operation for hexadecane steam reforming. The H_2O/C molar ratio was 2.7, with an operating temperature of 800 °C. When non-noble metals are employed, deactivation takes place within 8 h with less H_2 in the products under most reaction severities [7,11,12]. Kim et al. [13] noted H_2 concentrations of 72–65% over a 53-h steady state operation with a magnesia–alumina-supported nickel catalyst (Ni/MgO–Al_2O_3) at a temperature of 900 °C, gas hourly space velocity (GHSV) of 10 000 h^{-1} and an H_2O/C molar ratio of 3. They also reported lower deactivation rates when a noble metal (Rh) was added to the catalyst.

1.2. Reactor design

Since the reforming reactions are fast (high space velocities), reactor design is critical when liquid hydrocarbons have to be fed. The two major constraints are (a) as complete as possible mixing of the reactants (hydrocarbons and water) prior to entrance in the reaction zone, and (b) liquid pre-heating/vaporization/gas pre-heating of the reactants under such conditions that undesirable carbon forming cracking reactions might not take place to a significant extent. Hydrocarbons are not miscible with water, and if the above mentioned constraints are not respected, hydrocarbons pyrolysis occurs prior to the reaction in the pre-heating section [14]. Two reactor feeding methods have been described in the literature [14–17]: vaporization and atomization. When diesel is atomized, thermal cracking reactions are limited. By decreasing the size, and therefore increasing the surface of each droplet, better water/hydrocarbon mixing is reached prior to heating. Better pre-mixing of the reactants lowers thermal cracking reaction occurrence [14]. The usual means adopted for this purpose are ultrasound-enhanced or other commercial diesel engine injectors [14,16].

2. Materials and methodology

In the reported tests, the reactor exit concentrations of H_2, CO, CO_2 and CH_4 were compared to theoretical thermodynamic equilibrium concentrations, to determine if equilibrium was reached. Thermodynamic equilibrium concentrations were calculated with FactSage software on the basis of Gibbs energy minimization.

2.1. Catalyst preparation and analysis

The $NiAl_2O_4/Al_2O_3$–YSZ catalyst tested in this work was produced by the wet impregnation method. Al_2O_3 and YSZ (Y_2O_3–ZrO_2) (50–50%) support was prepared by mixing the two powders mechanically. Two Al_2O_3 powder sizes were studied: $NiAl_2O_4/Al_2O_3$–YSZ-1 at 20–40 nm, and $NiAl_2O_4/Al_2O_3$–YSZ-2 at 40 μm. YSZ powder size distribution had an upper limit at 20 μm. The Al_2O_3 and YSZ powder was impregnated with a $Ni(NO_3)_2{\cdot}6H_2O$ aqueous solution (for 5% weight nickel (Ni) load in the final formulation). Water was evaporated, and the resulting impregnated powder dried overnight at 105 °C. It was crushed-comminuted and calcined at 900 °C for 6 h to form the $NiAl_2O_4$ spinel. Catalysts were analyzed by scanning electron microscopy (SEM) Hitachi S-4700 Field Emission Gun and energy dispersive X-ray spectroscopy (EDXS) Oxford EDXS detector with an ultra-thin window ATW2.

2.2. Reforming

Propane reforming was undertaken for preliminary testing of the catalysts. Propane was chosen because it is the simpler saturated hydrocarbon containing carbon linked chemically with two other carbon atoms. Hexadecane reforming and tetralin reforming were performed to test the catalyst with paraffin and aromatic compounds. Hexadecane was chosen as a surrogate of diesel's paraffinic compounds while tetralin was selected as a representative of diesel's naphthenic and aromatic part.

A schematic of the reactor is presented in Fig. 1. Reactor inner diameter was 46 mm, and catalytic bed length was 60 mm. The catalyst in powder form is dispersed in quartz wool. The quartz wool is then compacted in the reactor to form a catalytic bed of quartz fiber containing catalyst particulates. Since the flow entering the bed comes from the injection device, it is highly turbulent and has no enough time to become fully developed. This configuration prevents channeling issues and helps obtaining a uniform catalytic bed with the small amount of catalyst used. In the case of propane reforming, gaseous propane was mixed with 110 °C steam

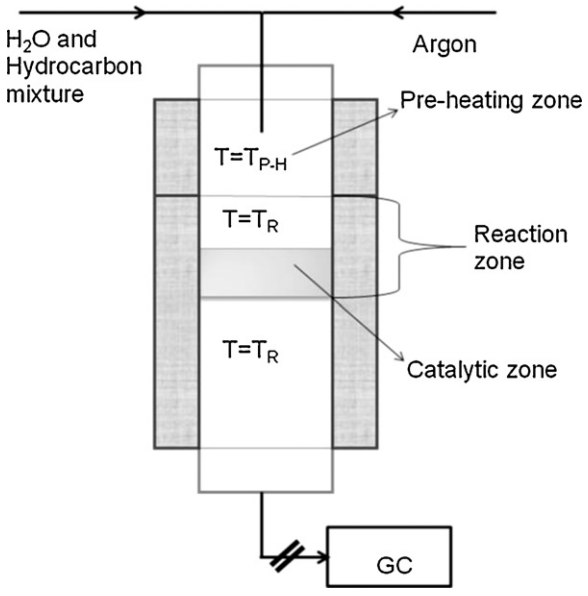

Fig. 1. Schematic of the steam reforming reactor for liquid hydrocarbons.

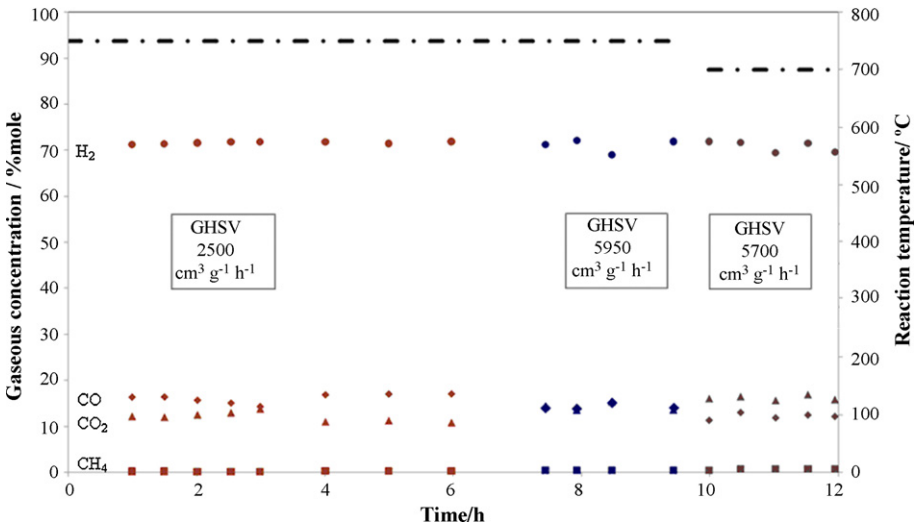

Fig. 2. Steam reforming of propane at different temperatures and GHSV with $H_2O/C = 3$.

before entering the pre-heating zone, which was maintained at 750 °C. In case of hexadecane and tetralin reforming, the emulsion, as explained below, entered at room temperature and was rapidly heated in the pre-heating zone maintained at 500 °C. The temperature just before the catalyst bed is between 30 °C and 45 °C below the reaction temperature, depending upon the operating parameters. The measured temperatures for the hexadecane and tetralin reforming experiments with $NiAl_2O_4/Al_2O_3$–YSZ-2 catalyst are indicated in the results section. Argon served as inert diluant and internal standard for liquid hydrocarbon steam reforming.

Propane was reformed in the packed-bed reactor (PBR) described above. The reactor was heated to the desired temperature under an argon (Ar) blanket. Ar flow was switched off prior to feeding the reactants. The reaction temperatures tested were 750 °C and 700 °C; pressure was barometric or slightly higher due to pressure loss along the PBR set-up, and the H_2O/C molar ratio was 3. The GHSV was between 2900 and 5950 $cm^3_{reac}\, g^{-1}_{cat}\, h^{-1}$ under reaction conditions.

The method chosen to enhance hydrocarbon/water mixing was the formation of an emulsion of two immiscible reactants in a surfactant-aided protocol. This emulsion was heated and vaporized before reaching the catalyst. The PBR described above with the catalyst dispersed in quartz wool was used for hexadecane reforming. H_2O/C was 2.5 for hexadecane reforming and 2.3 for tetralin reforming. The operating temperature was between 630 °C and 720 °C with GHSV ranging from 1900 to 12 000 $cm^3_{reac}\, g^{-1}_{cat}\, h^{-1}$ at barometric pressure. Reforming products were analyzed in a Varian CP-3800 gas chromatograph. The exit gaseous flow rate was measured using a mass flow rate mass meter (Omega FMA-700A).

2.3. Conversion calculations

Overall conversion was calculated for liquid hydrocarbon reforming based on the total amount of carbon fed in the reactor. Hydrocarbons were considered to be converted when they were transformed into gaseous products (CO, CO_2 or CH_4). The carbon found in the reactor after the experiment was therefore not considered as converted hydrocarbon. The following equation (Eq. (3)) was applied:

$$X = \frac{N_{CO_{out}} + N_{CO_{2_{out}}} + N_{CH_{4_{out}}}}{N_{C_mH_{n_{in}}} \times m + N_{Surfactant_{in}} \times Y} \quad (3)$$

N being the total number of moles, and Y, the number of carbon atoms in the surfactant.

Table 1
Gaseous concentrations measurement errors.

Gas	Standard gaseous concentration (%)	Absolute error (on % concentration of the standard)	Relative error (%)
H_2	55.16	0.46	0.83
CO	19.70	0.21	1.05
CO_2	6.96	0.38	5.45
CH_4	2.08	0.04	1.87
Ar	16.10	0.22	1.37

3. Results

3.1. Measurement errors

Errors associated with concentration data obtained by gas chromatography (GC) are presented in Table 1. They were calculated by using an external standard.

In addition to the GC concentrations measurement errors, the mass flow meter used to measure the exit gas flow introduces a second error in the conversion calculations. The accuracy of the mass flow meter is 1%. Maximum and minimum values were therefore calculated for each conversion, using the extreme values for concentrations and flow rate based on the known error and accuracy.

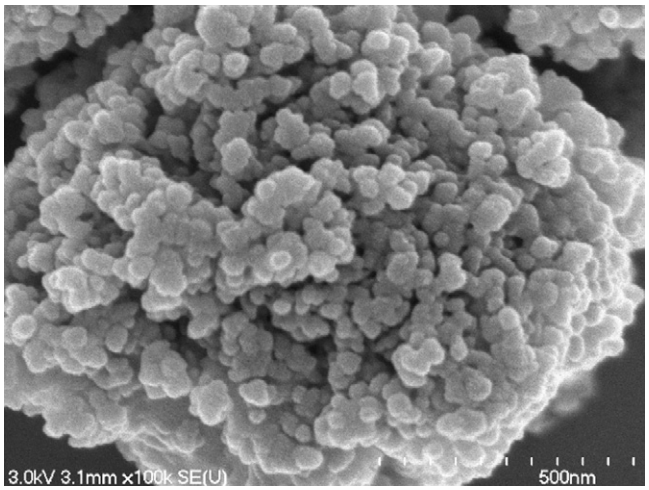

Fig. 3. SEM picture of the fresh $NiAl_2O_4/Al_2O_3$–YSZ-1 catalyst.

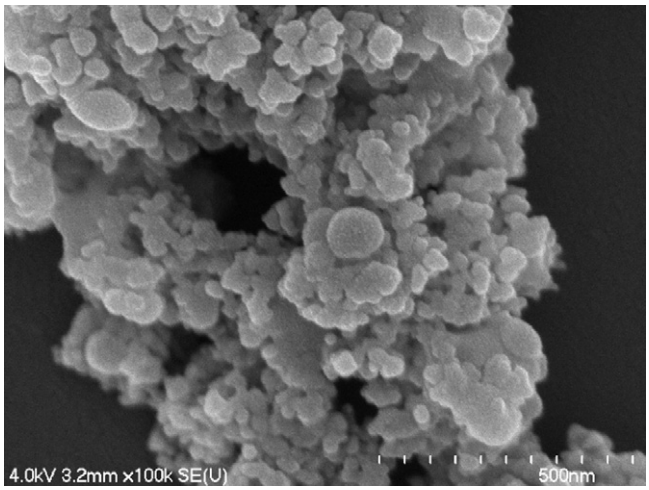

Fig. 4. SEM picture of the $NiAl_2O_4/Al_2O_3$–YSZ-1 catalyst after propane reforming.

3.2. Propane catalytic steam reforming with the $NiAl_2O_4/Al_2O_3$–YSZ-1 catalyst

The results of propane steam reforming with the $NiAl_2O_4/Al_2O_3$–YSZ-1 catalyst are presented at Fig. 2. During the first 10 h of reaction, the temperature was kept constant at 750 °C. For the last 2 h, it was decreased to 700 °C. The observed H_2 concentration was constant at 70% for the 12 h of operation, and methane concentration was below 1% for the entire reaction time. There was no deactivation of the catalyst. The shift in carbon monoxide and carbon dioxide concentrations with the decrease in temperature followed the predictions of theoretical thermodynamic equilibrium calculations. During the first 6 h of reactions a variation in the CO and CO_2 concentrations has been observed. This is due to the variability of the process over time and the measurements error. However, the gaseous concentrations are near those predicted by the theoretical thermodynamic equilibrium calculations.

SEM pictures of the catalyst before and after 12 h of reaction are shown in Figs. 3 and 4, respectively. No carbon deposition on the catalyst was evident. The somewhat larger catalyst grains observed in Fig. 4 were explained by some sintering activity which was not, nevertheless, sufficient to lower activity under reaction conditions. These results being positive, the catalyst was then tested on hexadecane steam reforming.

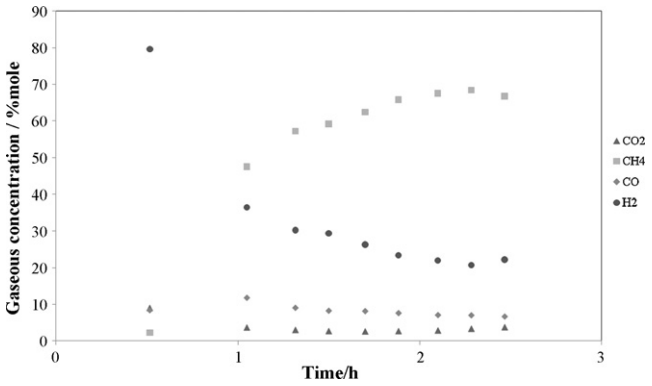

Fig. 5. Thermal cracking of hexadecane with $H_2O/C = 2.5$.

Table 2
Thermal cracking of hexadecane with $H_2O/C = 2.5$: Gas product composition at 25 °C .

Product	Gaseous concentration (% mole)
CO_2	1.4
CO	3.2
H_2	8.1
CH_4	19.7
C_2H_4	46.2
C_2H_6	4.5
C_3H_8	15.4
C_4H_{10}	1.5

3.3. Hexadecane catalytic steam reforming with the $NiAl_2O_4/Al_2O_3$–YSZ-1 catalyst

The results of a blank experiment are illustrated in Fig. 5. This blank experiment was performed without catalyst but with quartz wool as inert bed in the PBR, at a temperature of 710 °C and a flow rate of 22 700 $cm^3\ h^{-1}$. The concentrations corresponded to cracking, and no reforming reaction took place in the reactor without the catalyst. A major part of hexadecane was transformed into coke in the reactor, and conversion (as defined in Eq. (3)) was only 25%. In addition to this blank experiment, an experiment at 650 °C has been done aimed at measuring the concentration of the gas just before entering the catalytic zone. The concentrations of the gaseous products (at 25 °C) are presented in Table 2. The conversion as defined by Eq. (3) was only of 6%. The hexadecane conversion including the

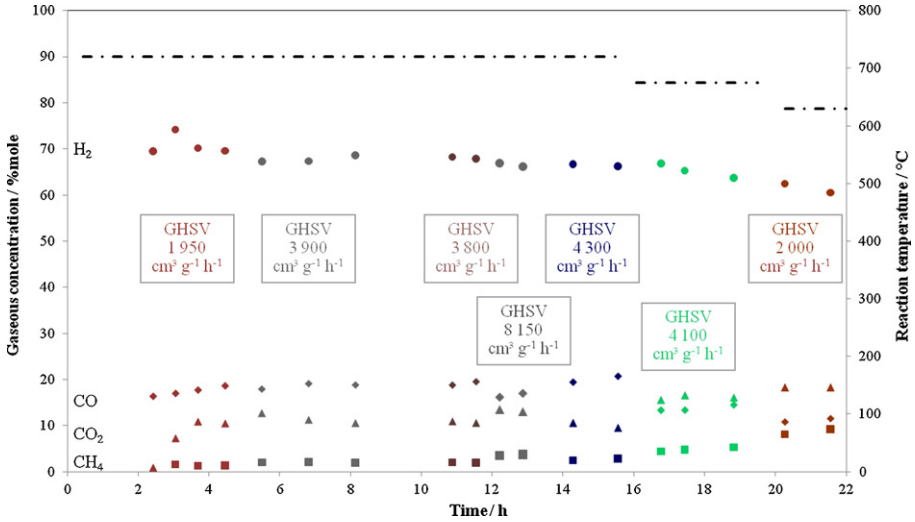

Fig. 6. Steam reforming of hexadecane at different temperatures and GHSV with $NiAl_2O_4/Al_2O_3$–YSZ-1 catalyst.

Table 3
Operating conditions for hexadecane steam reforming with the $NiAl_2O_4/Al_2O_3$–YSZ-2 catalyst.

Experiment	GHSV ($cm^3\ g^{-1}\ h^{-1}$)	Entrance temperature (°C)	Reaction temperature (°C)	H_2O/C ratio
1	5,000	655	710	2.5
2	4,800	648	670	2.5
3	12,000	645	670	2.5

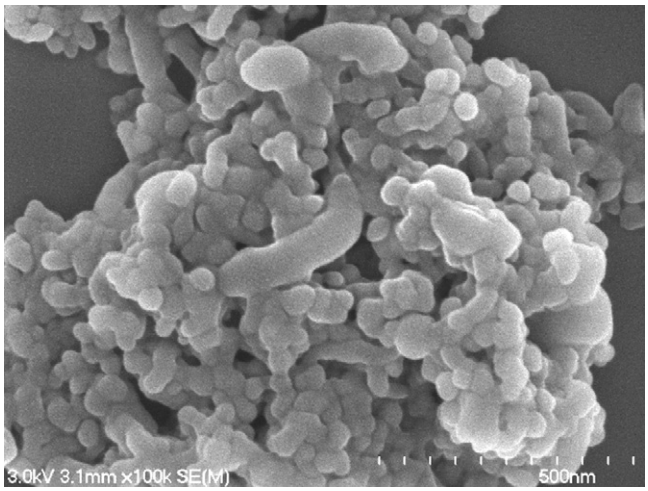

Fig. 7. SEM picture of the $NiAl_2O_4/Al_2O_3$–YSZ-1 catalyst after hexadecane reforming.

ethane, ethylene, propane and butane in the calculation was 42%. The rest of the reactants were collected as condensed liquid phase at the exit of the reactor.

The results of hexadecane steam reforming with the $NiAl_2O_4/Al_2O_3$–YSZ-1 catalyst are presented in Fig. 6. The catalyst was used for 22 h under different GHSV and three different temperatures, 720 °C, 675 °C, and 630 °C, with an H_2O/C ratio of 2.5.

Surface SEM analysis of the catalyst is reported in Fig. 7. As in the propane reforming test, there was no carbon deposition. The extent of sintering seemed to be higher. This could be linked to longer test durations (22 h instead of 12 h for propane), but since the temperature was lower, it was rather difficult to draw safe conclusions based only on these preliminary qualitative findings. However, no deactivation of the catalyst was due to this small extent of sintering.

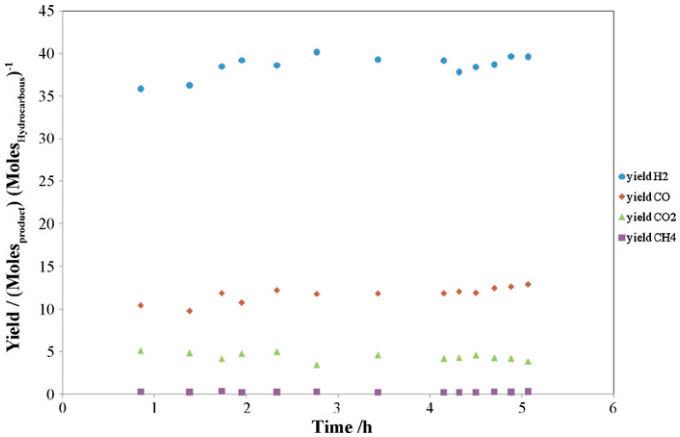

Fig. 8. Experiment 1: steam reforming of hexadecane with the $NiAl_2O_4/Al_2O_3$–YSZ-2 catalyst (GHSV = 5000 $cm^3\ g^{-1}\ h^{-1}$; T = 710 °C; H_2O/C = 2.5).

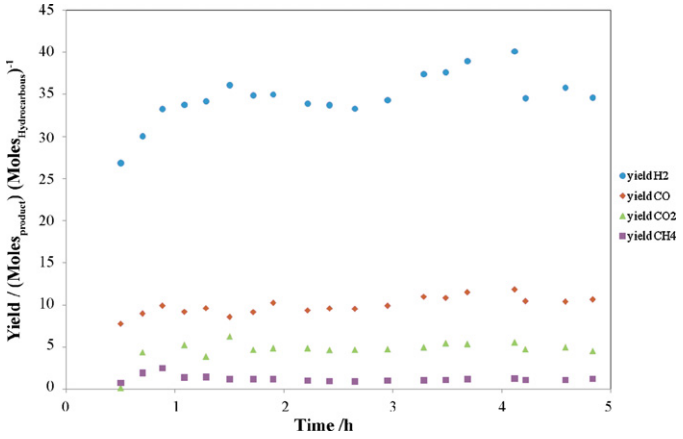

Fig. 9. Experiment 2: steam reforming of hexadecane with the $NiAl_2O_4/Al_2O_3$–YSZ-2 catalyst (GHSV = 4800 $cm^3\ g^{-1}\ h^{-1}$; T = 670 °C; H_2O/C = 2.5).

3.4. Hexadecane catalytic steam reforming with the $NiAl_2O_4/Al_2O_3$–YSZ-2 catalyst

The results of three experiments on hexadecane steam reforming with the $NiAl_2O_4/Al_2O_3$–YSZ-2 catalyst are reported in Figs. 8–10. The catalyst was tested under three different sets of operating conditions reported in Table 3.

It can be observed from experiments 1–3 (Figs. 8–10) that the concentrations at the exit gas were stable and consequently there was no catalyst deactivation observed. However, there was a slight difference in the concentrations of experiments 2 and 3, even if they were performed at the same temperature. This indicates that an increase of the GHSV from 5000 $cm^3\ g^{-1}\ h^{-1}$ to 12 000 $cm^3\ g^{-1}\ h^{-1}$ at a temperature of 670 °C had an effect on the reaction. In addition, conversion decreased at the higher GHSV. The calculated conversions are presented in Table 4. The difference in calculated conversions between experiments 1 and 2 is of the order of magnitude of the systematic error associated with the measurements

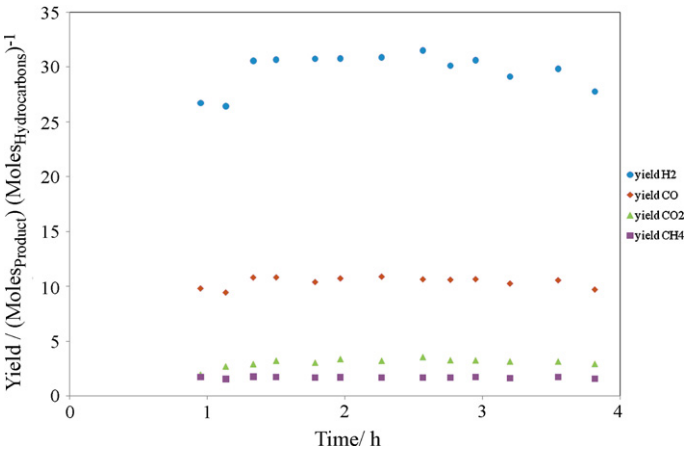

Fig. 10. Experiment 3: steam reforming of hexadecane with the $NiAl_2O_4/Al_2O_3$–YSZ-2 catalyst (GHSV = 12 800 $cm^3\ g^{-1}\ h^{-1}$; T = 670 °C; H_2O/C = 2.5).

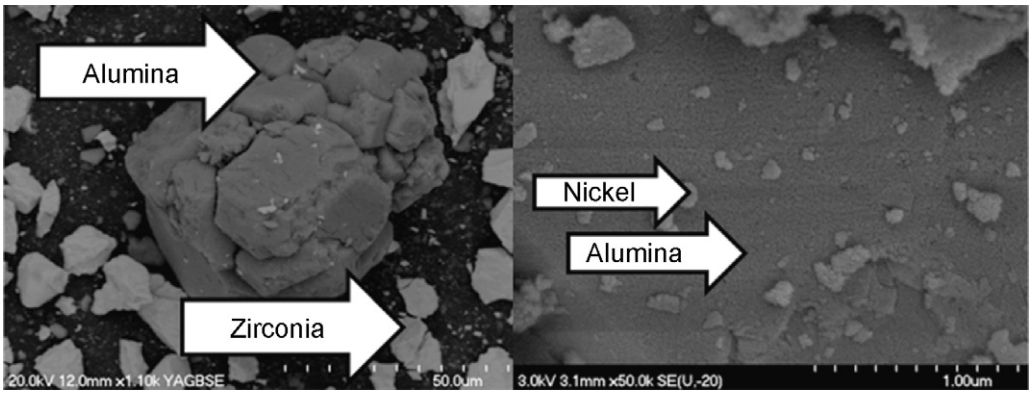

Fig. 11. SEM picture of the fresh $NiAl_2O_4/Al_2O_3$–YSZ-2 catalyst.

precision. The confidence intervals show that the conversion is statistically the same for both experiments. Moreover, as explained in Section 4, concentrations are at equilibrium. Finally, the decrease of temperature by 40 °C does not have a significant impact on conversion (comparison of experiments 1 and 2).

Surface SEM and SEM–EDX analyses of the fresh $NiAl_2O_4/Al_2O_3$–YSZ-2 catalyst are reported in Figs. 11 and 12. Fig. 12 shows that spinel catalyst support is composed of two types of distinct grains, those rich in alumina and those rich in YSZ. SEM–EDXS analysis of these two types of grains revealed that Ni was observable only on alumina grains.

SEM pictures of the catalyst after its use in experiments 1 and 3 are shown in Figs. 13 and 14, respectively. There is no apparent change in the morphology of the support and no sintering was observed.

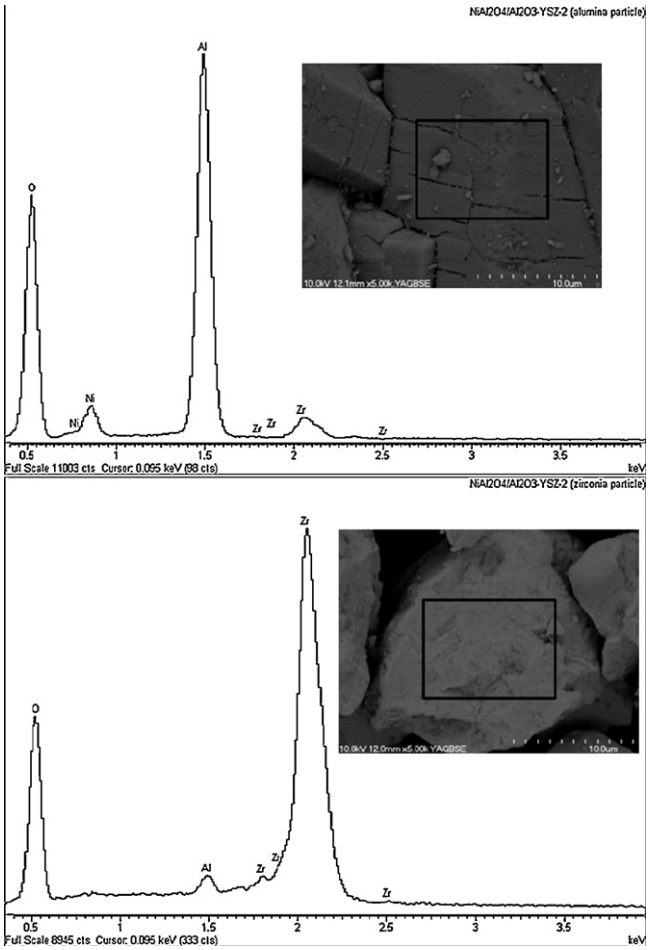

Fig. 12. SEM–EDXS of the fresh $NiAl_2O_4/Al_2O_3$–YSZ-2 catalyst.

SEM–EDXS analysis with the associated SEM picture of the $NiAl_2O_4/Al_2O_3$–YSZ-2 catalyst after its use in the three hexadecane experiments are shown in Figs. 15–17. Small quantities of graphitic carbon appear to be deposited only on the catalyst used in experiment 3; no carbon nanofibers were observed.

Fig. 18 presents the SEM–EDXS analysis of a catalyst made of metallic nickel deposited on the same substrate instead of the spinel. The mass compositions of the two catalysts were the same and the experiment took place at lower GHSV but all other operation conditions of experiment 3 were kept the same. The conversion was lower (0.76) and the analysis (Fig. 18) shows that there is a significant amount of carbon deposit on the catalyst including carbon nanofibers. This is a significant proof of the spinel's improved capacity to reform without favouring carbon formation and deposit.

Table 5 presents the BET analysis of the $NiAl_2O_4/Al_2O_3$–YSZ-2 catalyst before and after experiment 3. After the experiment, the catalyst was mechanically sorted out of its quartz wool matrix; however, some quartz wool remained with the catalyst. The quartz wool contribution in the BET analysis is insignificant (BET analysis

Table 4
Calculated conversions for hexadecane steam reforming with the $NiAl_2O_4/Al_2O_3$–YSZ-2 catalyst.

Experiment	Conversion
1	0.94 (0.908–0.970)
2	0.97 (0.938–0.996)
3	0.86 (0.839–0.889)

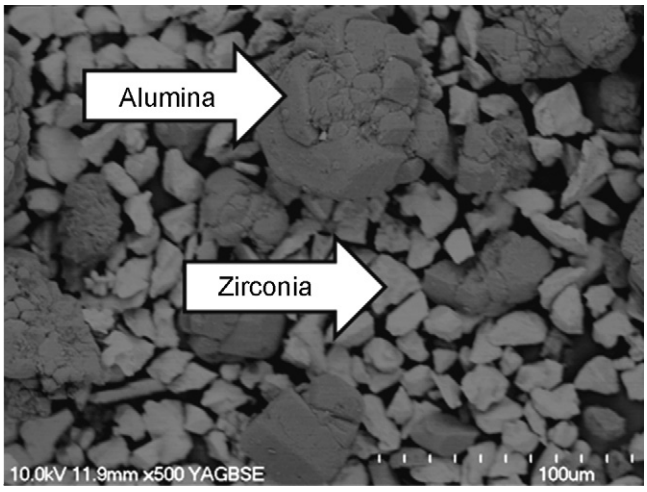

Fig. 13. SEM of the $NiAl_2O_4/Al_2O_3$–YSZ-2 catalyst (hexadecane – experiment 1).

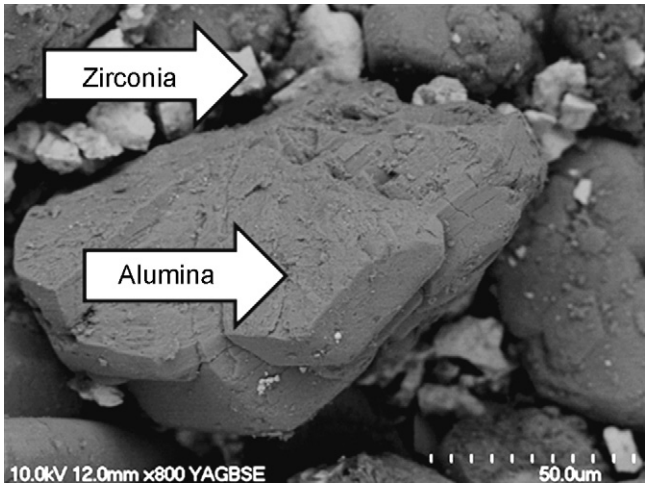

Fig. 14. SEM of the $NiAl_2O_4/Al_2O_3$–YSZ-2 catalyst (hexadecane – experiment 3).

of the quartz wool sample shows no measurable specific surface), but it is part of the mass of the sample. The results show that there is a relatively significant increase of the BET surface in the used catalyst. This leads to the conclusion that there is no measurable sintering; this fact is supported by the SEM analysis. At least a part of the BET specific surface increase can be attributed to catalyst grains breakage, also observed by SEM. Another part could be associated with the experimental error due to the possibility

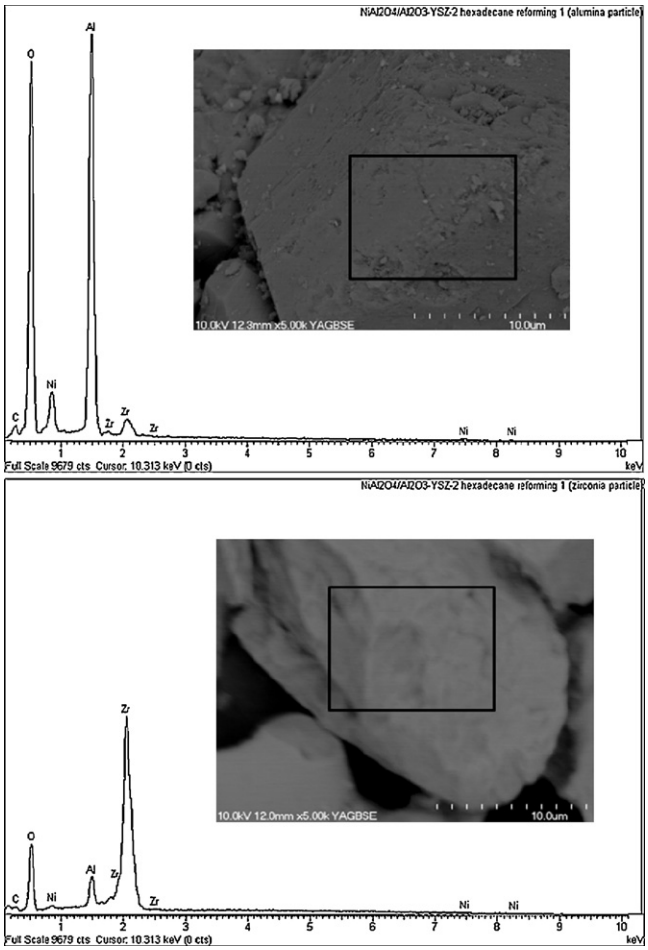

Fig. 15. SEM–EDXS of the $NiAl_2O_4/Al_2O_3$–YSZ-2 catalyst (hexadecane – experiment 1).

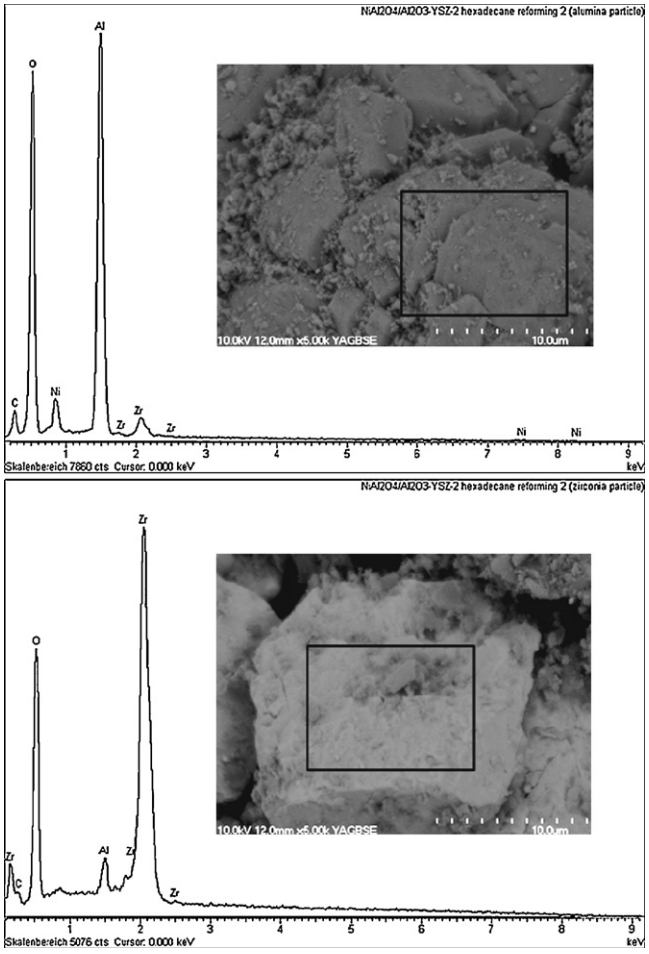

Fig. 16. SEM–EDXS of the $NiAl_2O_4/Al_2O_3$–YSZ-2 catalyst (hexadecane – experiment 2).

of having different quartz wool mass percentages in the measured samples.

3.5. Tetralin catalytic steam reforming with the $NiAl_2O_4/Al_2O_3$–YSZ-2 catalyst

The results obtained for tetralin steam reforming with the $NiAl_2O_4/Al_2O_3$–YSZ-2 catalyst are presented in Fig. 19. The catalyst was used under a GHSV of 4800 $cm^3\ g^{-1}\ h^{-1}$, an entrance temperature of 670 °C, a reaction temperature of 705 °C with an H_2O/C ratio of 2.3. The conversion obtained was 0.69 (0.668–0.715), explained by the higher refractory behaviour of cyclic/aromatic compounds in reforming reactions. Gaseous concentrations at the exit were, however, stable, with no deactivation of the catalyst. The BET surface of the catalyst after the experiment was 40.0 $m^2\ g^{-1}$, which is consistent with the observed behaviour in hexadecane reforming.

SEM–EDXS analysis with the associated SEM picture of the $NiAl_2O_4/Al_2O_3$–YSZ-2 catalyst after use in the tetralin experiment is shown in Fig. 20. There is no significant carbon deposition, and the results are similar to those obtained with the hexadecane reforming at similar conditions (experiment 2).

Table 5
BET surface area analysis of the $NiAl_2O_4/Al_2O_3$–YSZ-2 catalyst.

Catalyst	BET ($m^2\ g^{-1}$)
Fresh	35.0
After experiment 3	44.8

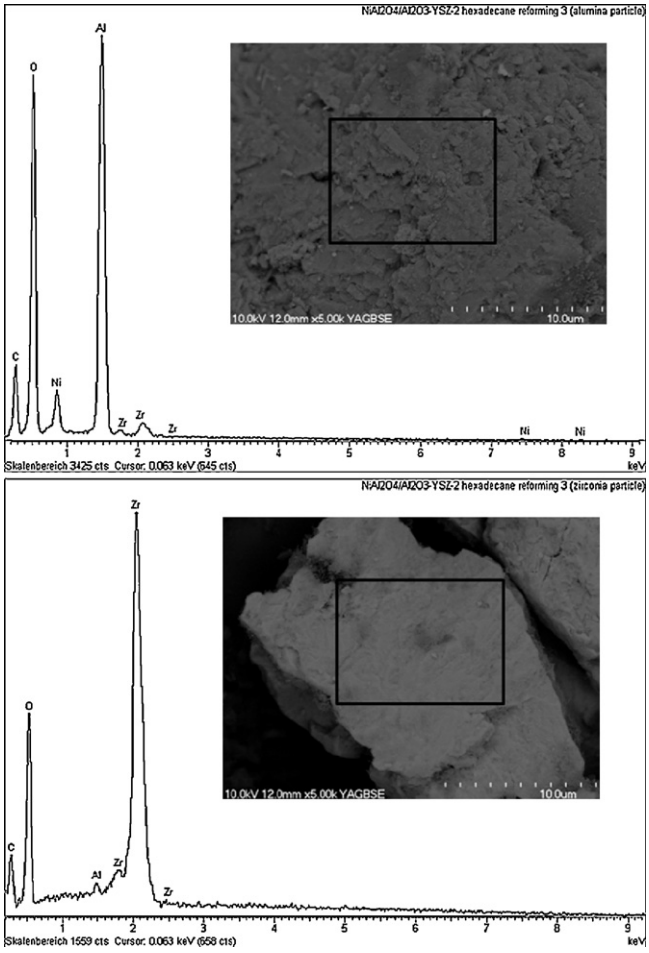

Fig. 17. SEM–EDXS of the $NiAl_2O_4/Al_2O_3$–YSZ-2 catalyst (hexadecane – experiment 3).

4. Discussion

For hexadecane steam reforming with the $NiAl_2O_4/Al_2O_3$–YSZ-1 catalyst, and for the entire duration of the reaction, the concentrations of H_2, CO, CO_2 and CH_4 were all near the values predicted from theoretical thermodynamic equilibrium calculations. Product concentrations were still close to equilibrium, even if lower temperatures decreased the rate of reforming reactions and thermodynamically favoured carbon formation and deposition through the Boudouard reaction. The equilibrium concentrations for hexadecane steam reforming appear in Fig. 21.

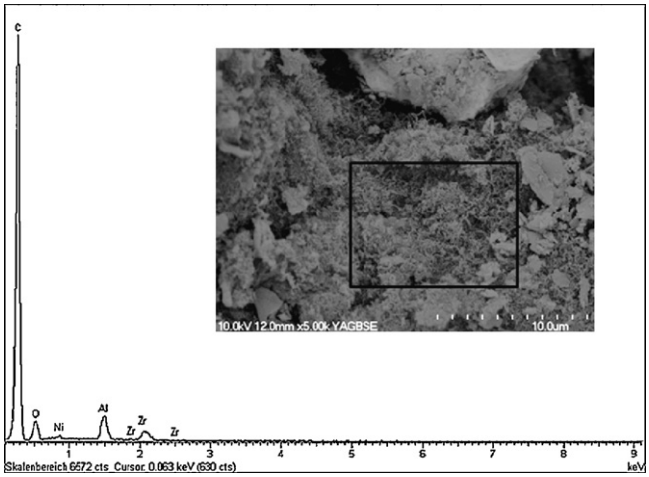

Fig. 18. SEM–EDXS of the Ni/Al_2O_3–YSZ catalyst (hexadecane reforming).

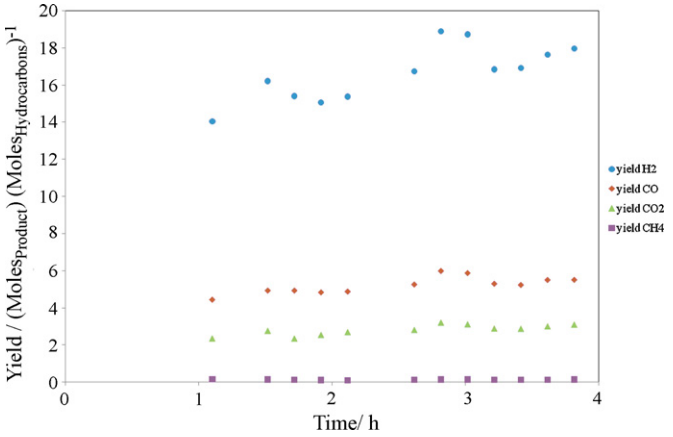

Fig. 19. Steam reforming of tetralin with the $NiAl_2O_4/Al_2O_3$–YSZ-2 catalyst (GHSV = 4800 $cm^3\ g^{-1}\ h^{-1}$; T = 705 °C; H_2O/C = 2.3).

Comparisons between theoretical equilibrium concentrations and experimental concentration are shown in Fig. 22 for hexadecane and Fig. 23 for tetralin with the $NiAl_2O_4/Al_2O_3$–YSZ-2 catalyst. It can be seen that the experimental concentrations were similar to theoretical equilibrium concentrations. For experiment 3, at higher GHSV, the concentrations were slightly different; these conditions were thus considered as the limit to operate within equilibrium conditions.

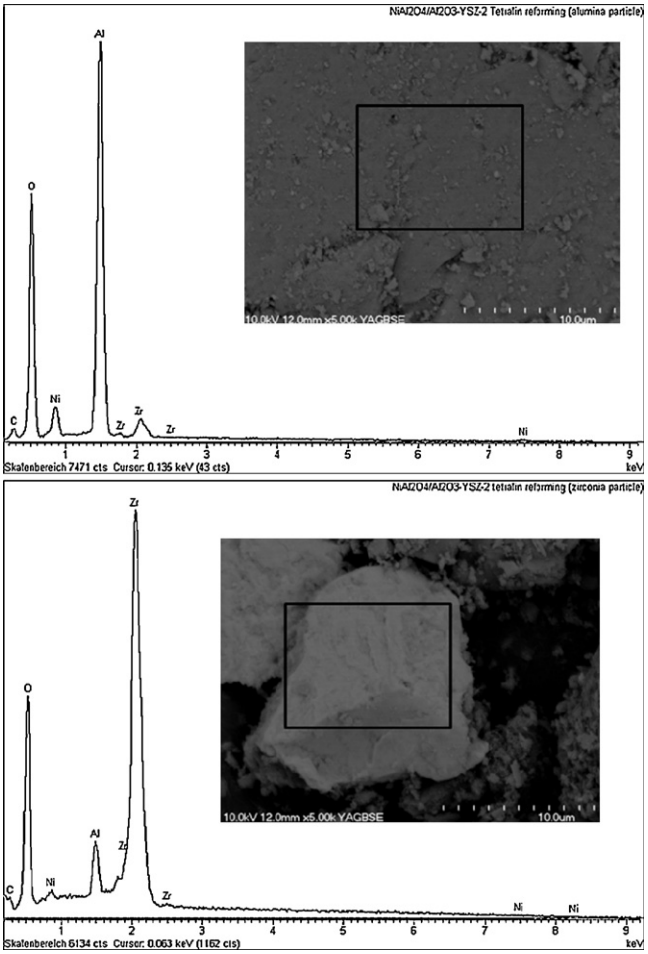

Fig. 20. SEM–EDXS of the $NiAl_2O_4/Al_2O_3$–YSZ-2 catalyst (tetralin).

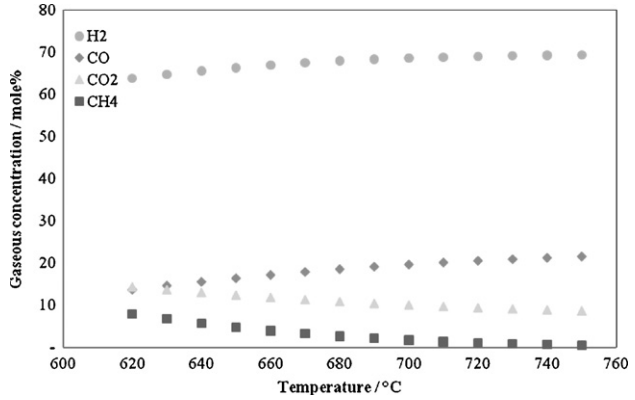

Fig. 21. Equilibrium concentrations of hexadecane steam reforming with molar $H_2O/C = 2.5$.

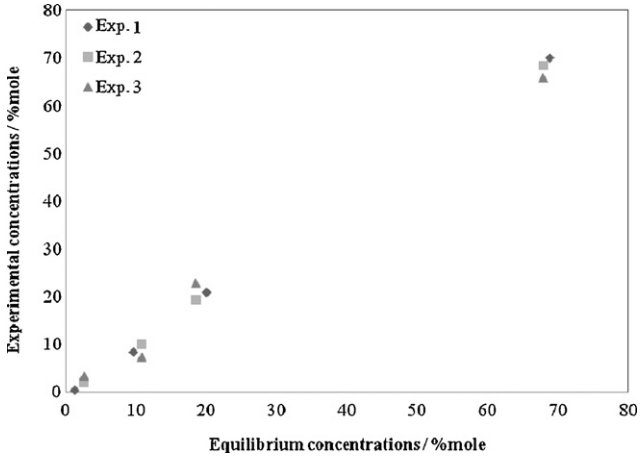

Fig. 22. Comparison of equilibrium and experimental concentrations for hexadecane steam reforming with the $NiAl_2O_4/Al_2O_3$–YSZ-2 catalyst.

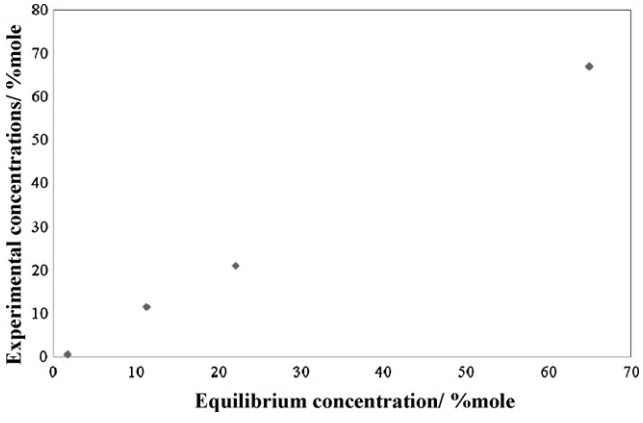

Fig. 23. Comparison of equilibrium and experimental concentrations for tetralin steam reforming with the $NiAl_2O_4/Al_2O_3$–YSZ-2 catalyst.

5. Conclusions

This work proposes a new formulation based on a Ni–alumina spinel supported on an Al_2O_3–YSZ ceramic matrix as a liquid hydrocarbon (diesel surrogate) steam reforming catalyst. Testing was performed in an isothermal PBR, and catalyst evaluation included its performance at various reaction severities under theromodynamic or near thermodynamic equilibrium conditions. Reactants feeding as a stabilized hydrocarbon–water emulsion proved to be efficient and prevented undesired pre-cracking. The $NiAl_2O_4/Al_2O_3$–YSZ-1 and $NiAl_2O_4/Al_2O_3$–YSZ-2 catalysts gave high conversion and high H_2 concentrations. There was no significant coking on the active part of the catalysts, even at high reaction severities. Moreover, product concentrations were close to equilibrium and constant over time for durations up to about 20 h. Regarding operating conditions, the GHSV for reaching equilibrium were equal to or higher than those found in the literature at equal or higher reaction severities (temperature). The use of different particle size supports does not seem to have a significant effect on activity, but this, as well as testing with real diesel at various reaction severities, is under study.

Acknowledgements

The authors are indebted to SOFC-Canada Network, the National Science and Engineering Research Council of Canada (NSERC) and the Fonds québécois de recherche sur la nature et les technologies (FQRNT) for funding related to this project. The technical contributions of Henri Gauvin in the reforming tests rig and Stéphane Gutierrez in SEM/EDX catalyst characterization are highly appreciated. Special thanks to Mr. Ovid Da Silva for reviewing this manuscript.

References

[1] A.F. Ibarreta, C. Sung, Int. J. Hydrogen Energy 31 (8) (2006) 1066–1078.
[2] D.N. Bangala, N. Abatzoglou, E. Chornet, AIChE J. 44 (4) (1998) 927–936.
[3] J. Blanchard, A.J. Nsungui, N. Abatzoglou, F. Gitzhofer, Can. J. Chem. Eng. 85 (2007) 889–899.
[4] L. Oukacine, F. Gitzhofer, N. Abatzoglou, D. Gravelle, Surf. Coat. Technol. 201 (5) (2006) 2046–2053.
[5] K. Lucka, H. Kohne, Clean Air 7 (4) (2006) 381–390.
[6] Q. Ming, T. Healey, L. Allen, P. Irving, Catal. Today 77 (1–2) (2002) 51–64.
[7] M.C. Alvarez-Galvan, R.M. Navarro, F. Rosa, Y. Briceno, F. Gordillo Alvarez, J.L.G. Fierro, Int. J. Hydrogen Energy 33 (2) (2008) 652–663.
[8] P.K. Cheekatamarla, A.M. Lane, J. Power Sources 152 (1–2) (2005) 256–263.
[9] F. Rosa, E. Lopez, Y. Briceno, D. Sopena, R.M. Navarro, M.C. Alvarez-Galvan, J.L.G. Fierro, C. Bordons, Catal. Today 116 (3) (2006) 324–333.
[10] J.J. Strohm, J. Zheng, C. Song, J. Catal. 238 (2) (2006) 309–320.
[11] T.H. Gardner, D. Shekhawat, D.A. Berry, M.W. Smith, M. Salazar, E.L. Kugler, Appl. Catal. A 323 (2007) 1–8.
[12] B.D. Gould, A.R. Tadd, J.W. Schwank, J. Power Sources 164 (1) (2007) 344–350.
[13] D.H. Kim, J.S. Kang, Y.J. Lee, N.K. Park, Y.C. Kim, S.I. Hong, D.J. Moon, Catal. Today 136 (2008) 228–234.
[14] D. Liu, M. Krumpelt, H. Chien, S. Sheen, J. Mater. Eng. Perform. 15 (4) (2006) 442–444.
[15] T. Aicher, L. Griesser, J. Power Sources 165 (1) (2007) 210–216.
[16] I. Kang, J. Bae, S. Yoon, Y. Yoo, J. Power Sources 172 (2) (2007) 845–852.
[17] A. Sarioglan, H. Olgun, M. Baranak, A. Ersoz, H. Atakul, S. Ozdogan, Int. J. Hydrogen Energy 32 (14) (2007) 2895–2901.